

Nanofluidic Traps by Two-Photon Fabrication for Extended Detection of Single Macromolecules and Colloids in Solution

Oliver Vanderpoorten,[∇] Ali N. Babar,[∇] Georg Krainer,[∇] Raphaël P. B. Jacquat,[∇] Pavan K. Challa, Quentin Peter, Zenon Toprakcioglu, Catherine K. Xu, Ulrich F. Keyser, Jeremy J. Baumberg, Clemens F. Kaminski, and Tuomas P. J. Knowles*



Cite This: <https://doi.org/10.1021/acsanm.1c03691>



Read Online

ACCESS |



Metrics & More



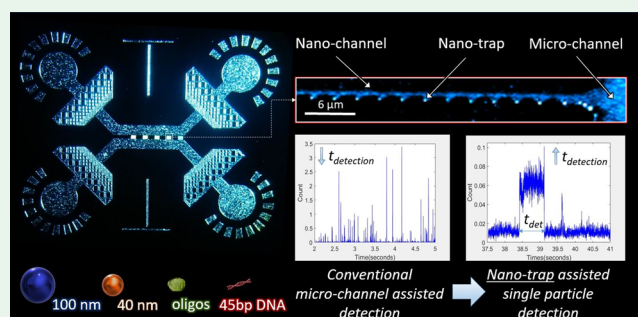
Article Recommendations



Supporting Information

ABSTRACT: The analysis of nanoscopic species, such as proteins and colloidal assemblies, at the single-molecule level has become vital in many areas of fundamental and applied research. Approaches to increase the detection time scales for single molecules in solution without immobilizing them onto a substrate surface and applying external fields are much sought-after. Here, we present an easy-to-implement and versatile nanofluidics-based approach that enables increased observational-time scale analysis of nanoscopic material building blocks such as single biomacromolecules and nanoscale colloids in solution. We use two-photon-based hybrid lithography in conjunction with soft lithography to fabricate nanofluidic devices with nanotrapping geometries down to 100 nm in height. We provide a rigorous description and characterization of the fabrication route that enables the writing of nanoscopic 3D structures directly in photoresist and allows for the integration of nanotrapping and nanochannel geometries within microchannel devices. Using confocal fluorescence burst detection, we validated the functionality of particle confinement in our nanotrap geometries through measurement of particle residence times. All species under study, including nanoscale colloids, α -synuclein oligomers, and double-stranded DNA, showed a 3- to 5-fold increase in average residence time in the detection volume of nanotraps, due to the additional local steric confinement, in comparison to free space diffusion in a nearby microchannel. Our approach thus opens up the possibility for single-molecule studies at prolonged observational-time scales to analyze and detect functionalized nanoparticles and protein assemblies in solution without the need for surface immobilization.

KEYWORDS: nanoparticle trapping, nanofluidics, 2-photon lithography, protein oligomers, DNA, molecular trapping, confocal fluorescence detection, soft lithography



INTRODUCTION

The spatial confinement of biomolecules or colloidal nanoparticles in solution for biophysical studies at the single-molecule level has become instrumental in many areas of fundamental and applied research including nanobiotechnology,¹ biophysics,² and clinical diagnostics.³ It allows for increased observational-time scale analysis of nanoscopic species such as nucleic acids, protein assemblies,⁴ or colloidal particles⁵ with single-molecule sensitivity.⁶ Improved nanoscopic single-molecule detection schemes are key for the development of new material building blocks on the nanoscale, which play an essential role in bottom-up assembly processes of meta materials,⁷ amyloid fibrils,⁸ and DNA origami technology⁹ as well as in nanoparticle synthesis and their surface functionalization.¹⁰ Currently, molecular confinement is most typically achieved through surface immobilization of the biomolecule or nanoparticle of interest on a substrate surface (e.g., for confocal or total internal reflection fluorescence (TIRF) microscopy).^{11–13} This approach, how-

ever, has numerous drawbacks, not least because surface interactions can change the molecule's configuration and function.

An alternative to surface immobilization is the trapping of particles in solution without immobilizing them onto a substrate surface. Various approaches using external fields, such as electric,¹⁴ hydrodynamic,¹⁵ and optical fields,^{16,17} for nanoparticle trapping in solution have emerged. Optical trapping, for example, has been proven to be effective in measuring repulsive or attractive forces between particles such as colloids and proteins, but the high laser powers required

Received: November 2, 2021

Accepted: November 24, 2021

induced flows around the trapped particles, leading to undesirable and confounding effects.¹ Furthermore, such techniques suffer from low throughput and require a refractive index mismatch between the particle and its surrounding media,¹⁸ which is often not the case when monitoring biological specimens. Other techniques, such as thermal trapping,^{19–21} have also been shown to be effective at confining nanoparticles in small volumes, but similar to optical trapping, thermal particle trapping has significant drawbacks due to the sample undergoing motion because of convection. This puts limitations on the estimation of particle properties such as molecular size and particle reaction kinetics at physiologically relevant conditions.

Recently, geometry-induced electrostatic trapping and colloidal trapping based on the spatial modulation of configurational entropy was demonstrated.^{22,23} This approach enables trapping without applying external fields and has been proven to be invaluable in observing particles in an all aqueous environment.²⁴ Mojarad and Krishnan²⁵ demonstrated trapping of colloids and gold nanoparticles in nanofluidic silica devices, which allowed measurement of their particle size and charge in silica-based nanowells. Ruggeri et al.^{26,27} further pushed the limits of nanotrapping-based electrometry to the single-molecule level. While efficient in their use, to date, the fabrication of such trapping devices and their subsequent integration with microfluidic device platforms is challenging and demands specialized clean room equipment such as electron beam lithography (EBL)²⁸ and reactive ion etching (RIE).²⁹ Even though such approaches generate nanoslits or nanochannels smaller than 100 nm,³⁰ the complexity of the fabrication process, writing times, and the costs to produce a single device render these techniques highly inefficient and impractical. Additionally, most of these techniques have relatively low throughput, and their integration with microchannels, which is required for the chip-to-world interface, can be challenging.

An alternative approach for fabricating nanotraps/nanochannels and integrating the nanostructures within a microfluidic chip platform involves the combination of conventional UV lithography followed by two-photon lithography (2PL),^{31,32} where a focused femtosecond pulsed laser is scanned across the photoresist, resulting in the writing of device features below 200 nm in lateral size. 2PL or direct laser writing (DLW) is a powerful emerging technology and has gained much attention in recent years for the fabrication of 3-dimensional (3D) micro- and nanostructures and functional devices below the diffraction limit.³³ The fabrication of arbitrary 3D structures is possible in a photoresist from computer-generated 3D models and thus constitutes a fast and straightforward fabrication procedure.³⁴ Previously, microfluidic,³⁵ nanofluidic,³⁶ and optofluidic³⁷ devices were fabricated using femtosecond laser 3D micromachining and were shown to allow for the integration of functionalities unachievable with conventional UV lithography in device designs.

Here, we demonstrate the facile fabrication of nanofluidic trapping devices using a 2PL system for increased observational-time scale single-molecule studies of biomacromolecules and colloids in solution. To this end, we developed an approach based on hybrid 2PL- and UV lithography in conjunction with soft lithography³⁸ to generate nanoscale channels and adjacent nanoscale trap structures with dimensions down to 100 nm in height in a single step from

a silicon master wafer. This allowed for the fabrication and prototyping of nanofluidic polydimethylsiloxane (PDMS)–silica devices in a facile and scalable manner and the writing of various nanotrapping geometry designs with varying heights in one writing process. We analyzed the master wafer and PDMS imprints using correlative scanning electron microscopy (SEM) and atomic force microscopy (AFM) characterization techniques and validated the functionality of particle confinement in nanotrap geometries through measurement of particle residence times in nanotraps as compared to microchannels using single-molecule fluorescence burst analysis. We found that all species analyzed, including nanoscale colloids, protein oligomers, and short DNA duplexes, showed a 3- to 5-fold increase in average residence time in the detection volume of nanotraps in comparison to free space diffusion in a nearby nano- or microchannel. We further demonstrate other fluorescence microscopy techniques (confocal imaging and TIRF microscopy) as alternative readout techniques to be used in combination with nanofluidic traps. Taken together, our developments presented herein constitute a cost-effective and easy-to-implement approach for the fabrication of nanofluidic trap devices and open up a broad avenue of possibilities to study single molecules in solution for extended periods of time without permanent surface immobilization and without applying external fields.

RESULTS AND DISCUSSION

Integration of Nanotrapping and Nanochannel Geometries between Microchannels with 2-Photon Lithography. Conventional fabrication of trapping devices relies on sophisticated clean room equipment²² and does not allow high throughput and flexibility in the writing of structures of varying geometry and height. To overcome these challenges and make the fabrication process more facile, we propose here a fabrication route of nanofluidic devices via hybrid 2PL that enables the writing of nanoscopic 3D structures directly in photoresist.³² By combining large area UV mask lithography with local high precision two-photon laser writing, we demonstrate the integration of nanotraps written adjacent to nanochannels in a pre-existing microfluidic device design (see Figure 1). Since 2PL is a dosage-dependent process and the smallest feature size obtained in the photoresist depends on

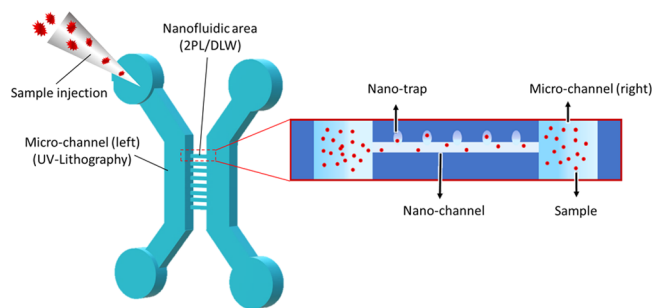


Figure 1. Design and fabrication of nanofluidic device with trapping functionalities. Schematic of the device design consisting of microfluidic reservoirs, inlets/outlets, nanofluidic channels, and nanotrapping arrays. 2-photon lithography (2PL) (or direct laser writing, DLW) is used to combine microfluidics with nanofluidic functionalities. Large area mask-based UV lithography patterns of microfluidic areas, whereas 2PL incorporates nanochannels and nanotraps in between two microchannels. The inset illustrates the placement of the nanotraps next to the nanofluidic channel.

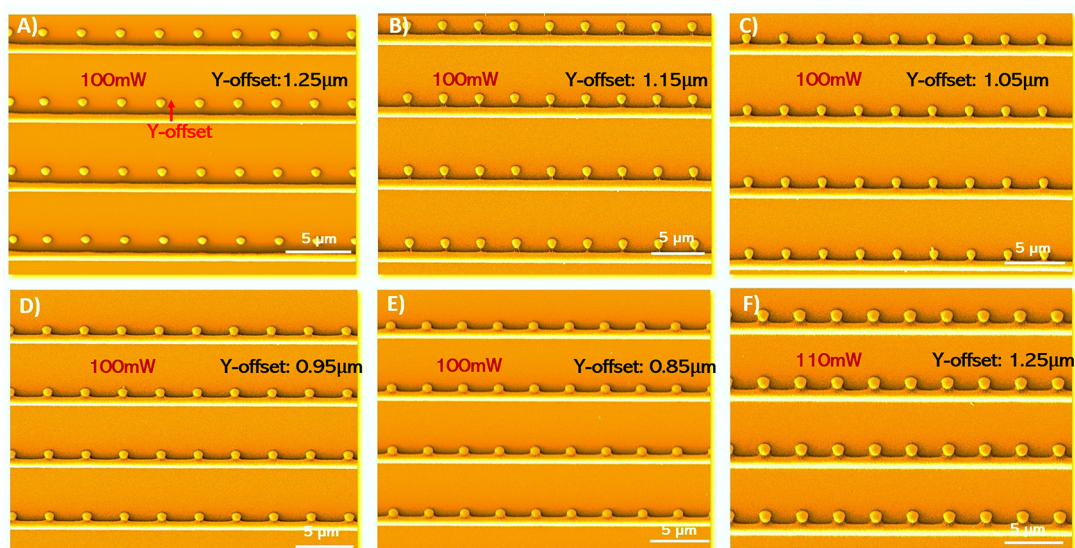


Figure 2. Prototypes of nanochannel and nanotrap geometries fabricated in photoresist using 2-photon lithography. Shown are SEM micrographs of nanochannel/nanotrap molds as obtained by 2-photon lithography in SU-8 photoresist using varying laser powers and Y-offsets. The writing speeds for the nanotraps and nanochannels were 1000 and 100 $\mu\text{m}/\text{s}$, respectively. (A–E) Nanochannel/nanotrap molds obtained with a Y-offset in the range of 1.25–0.85 μm ; the laser power for writing nanochannels and nanotraps was 90 and 100 mW, respectively. (F) Optimized nanochannel/nanotrap mold written with a Y-offset of 1.25 μm ; the laser power for writing nanochannels and nanotraps was 100 and 110 mW, respectively.

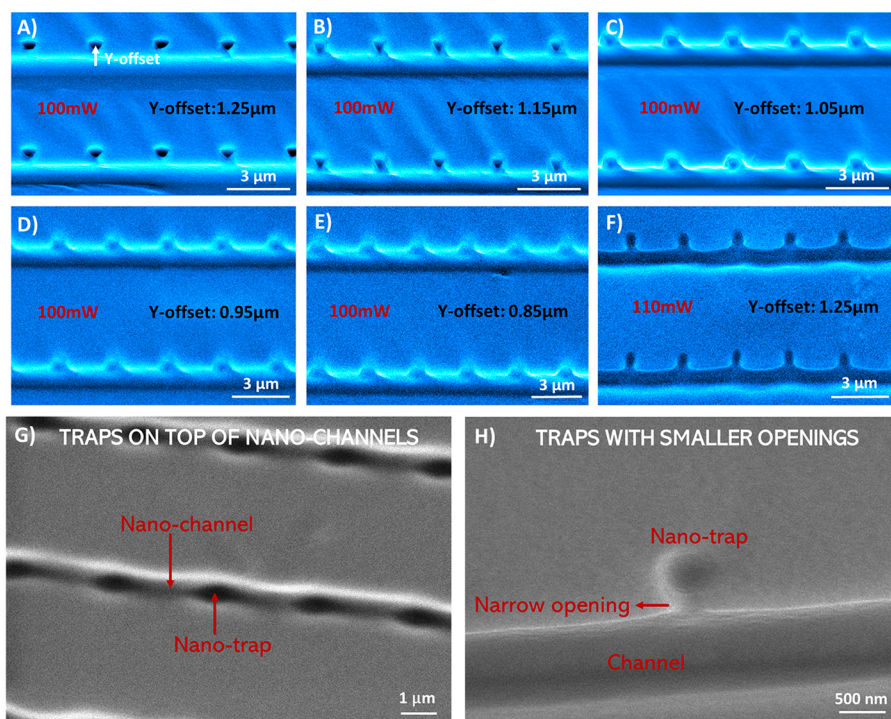


Figure 3. PDMS imprints of nanochannel and nanotrap device prototypes. Shown are SEM micrographs for the nanochannels and nanotraps imprinted in PDMS. The molds, from which the PDMS imprints were fabricated, were written in SU-8 photoresist with 2PL by varying the laser power and Y-offset (Figure 2). The writing speeds for the nanotraps and nanochannels were 1000 and 100 $\mu\text{m}/\text{s}$, respectively. (A–E) Nanochannels and nanotraps imprinted in PDMS with Y-offset in the range of 1.25–0.85 μm ; the laser power for the nanochannels and nanotraps was 90 and 100 mW, respectively. (F) Optimized nanochannel/nanotraps imprinted in PDMS with a Y-offset of 1.25 μm ; the laser power for the nanochannels and nanotraps was 100 and 110 mW, respectively. (G) SEM image of a trapping device with nanotraps on top of the nanochannels in the PDMS (top view). (H) SEM image of the narrow opening of a nanotrap imprinted in PDMS. Correlative AFM imaging showed a height of approximately 100 nm of the pockets (Figure S1).

the laser intensity and exposure time, we first set out to optimize the fabrication procedure to achieve fully merged nanotrap and nanochannel geometries.

We began by exploring and prototyping nanofluidic geometries in negative SU-8 photoresist (Figure 2) and produced imprints into PDMS following standard UV- and

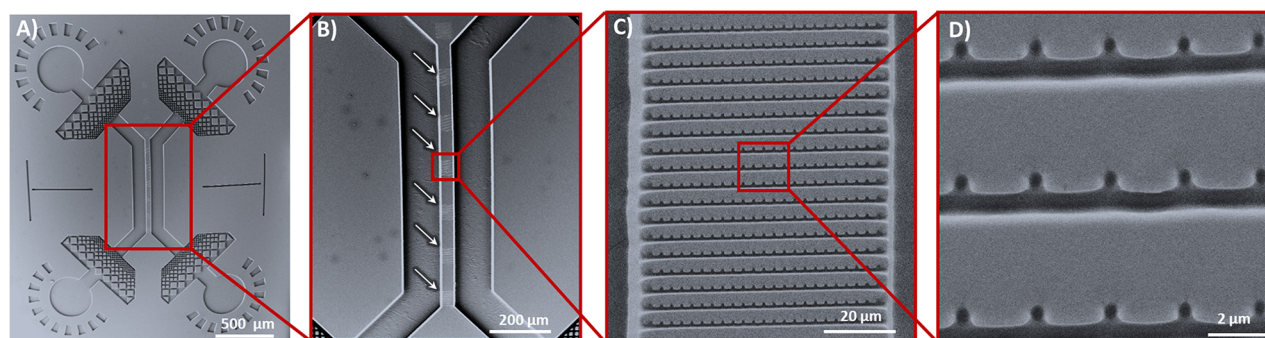


Figure 4. Nanofluidic device with trapping functionalities for single-molecule experiments. Shown are SEM micrographs of PDMS nanofluidic device imprints fabricated via hybrid UV mask lithography and 2PL. (A) Full view of the micro/nanofluidic device, consisting of microfluidic reservoirs, inlets/outlets, nanofluidic channels, and nanotrapping arrays. The design corresponds to the schematic shown in Figure 1. (B) Magnification depicting the arrays of 75 μm long nanochannels with integrated nanotraps in between the two 25 μm deep microchannels in PDMS. (C) The higher magnification of nanofluidic channels and nanotraps shows consistent imprinting of nanotrapping arrays in PDMS. (D) Zoom-in of the SEM micrograph showing the geometry of the nanotraps.

soft-lithography protocols (Figure 3). Characterization techniques such as SEM and AFM were used to analyze the prototype nanostructures. Variations in the laser power, laser writing speed, and the distance in between the nanotraps and nanochannel (Y-offset) during the 2PL writing process resulted in different configurations of nanotrap molds as shown in Figure 2A–E. Straight nanochannels were written at a fixed laser intensity of 90 mW and a writing speed of 100 $\mu\text{m}/\text{s}$. Dots for nanotrap molds were written adjacently with 1000 $\mu\text{m}/\text{s}$ scanning speed and by modulating the laser at 100 mW. Nanotraps were added every 3 μm along the nanochannels. The height of the nanotraps was smaller than the nanochannels due to the lower net exposure of the photoresist. Notably, the 3D piezo-flexure stage used for scanning the laser beam is a key component and allows one to vary the Y-offset between nanotraps and nanochannels with a resolution down to 10 nm by leveraging the closed-loop control mode of a piezo stage. Accordingly, the Y-offset was varied from 1.25 to 0.85 μm in steps of 100 nm. As shown in Figure 2B, at a Y-offset of 1.15 μm , the SU-8 of the nanotrap geometry merged with the nanochannel through monomer cross-linking. The same geometries were also analyzed in the PDMS imprints as shown in SEM micrographs of Figure 3A–E. Notably, when only the Y-offset between the nanochannel and nanotraps was varied, different geometries and designs of the nanotraps in PDMS could be generated, for example, triangular nanotraps as shown in Figure 3B. This highlights not only the importance of precise laser positioning to control the merge of nanochannels with nanotraps but also the possibility to create traps with varying geometries. The process of 2PL for writing almost arbitrary 3D structures thus allows significant flexibility here to choose and modulate the desired geometry and microfluidic chip design and introduce multiple geometry layers within a single spin-coating process. Indeed, we were able to add other conformations of traps to a nanochannel, for example, where the traps were positioned on top of the nanochannels (Figure 3G) or nanotraps with bottleneck openings (Figure 3H) on the side. The latter structures exhibited a nanotrap height of 100 nm, as confirmed by correlative SEM/AFM measurements on the master wafer (Figure S1).

The prototyping geometries obtained thus far were used to determine appropriate and optimized writing parameters to create the nanofluidic trapping devices required for nanoparticle and biomolecule trapping in single-molecule experi-

ments (see below). For this chip design, we required round nanotrapping cavities of a few hundred nanometers in radius, which are well-merged with straight nanochannels that have dimensions in the submicron regime. Such geometrical features could be obtained by using 110 mW laser power for writing of the traps, 100 mW for the nanochannels, and a Y-offset in between them of 1.25 μm (Figure 2F). Thereby, we fabricated nanotraps of 350 nm in radius adjacent to nanochannels of 650 nm in width. The chosen fabrication parameters show geometrical consistency between individual traps and are still mechanically stable enough to have the same structures in the final bonded device. The mechanical stability of the nanotrap structures in SU-8 was further enhanced by increasing the cross-linking density of monomers with a second UV exposure after writing nanostructures with 2PL.³⁹

Integration of Nanochannel and Nanotrap Geometries in a Microfluidic Device Platform. After having optimized the procedures for generating nanotrap and nanochannel geometries via our 2PL approach, we set out to fabricate the combined nanofluidic device for single-molecule experiments, as shown in Figure 1. The device was produced by first generating the micron-scale structures of the chip, which consisted of two microfluidic channels and reservoirs, sample inlets/outlets, and prefilters. This was done by transferring these chip features from a high-resolution transparency acetate photomask onto a SU-8 photoresist, spin-coated on a silicon wafer, via conventional contact UV lithography.³⁰ In the second step, the microfluidic channel reservoirs, separated by 75 μm , were connected with straight nanochannels and adjacent nanotraps using the optimized 2PL writing parameters, as detailed above (c.f., Figures 2F and 3F). Subsequently, PDMS imprints and glass-bonded chips were produced from these structures using standard soft lithography and replica molding procedures. Figure 4A shows a SEM micrograph of the final PDMS imprint with an overview of the conventional micron-scale chip functionalities. Further magnification (Figure 4B–D) shows the successful integration of nanofluidic functionalities in between the microfluidic reservoirs. Two microfluidic compartments of 25 μm depth were joined by 2PL with six nanofluidic areas (Figure 4B, indicated with arrows). Figure 4C shows in greater detail one nanotrapping array consisting of 18 nanochannels with adjacently added nanotraps every 3 μm . Notably, the channels show a wider funnel-like shape at the microfluidic interface due

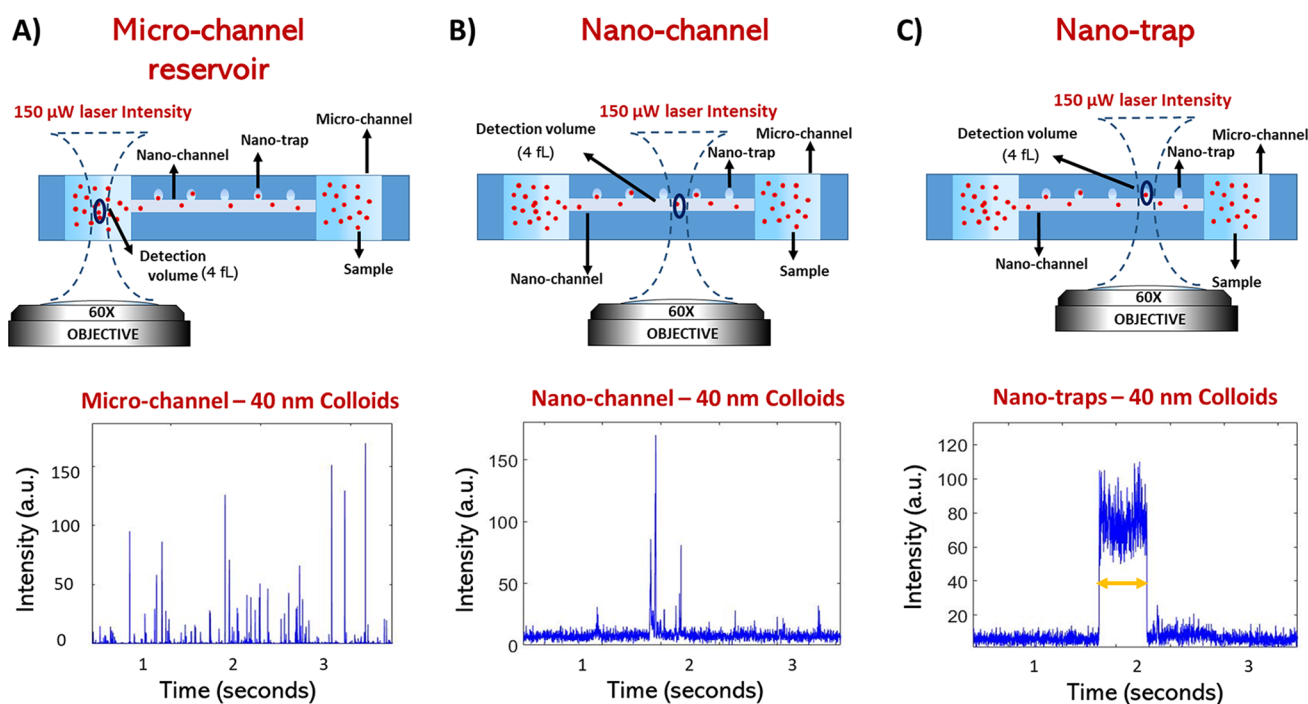


Figure 5. Single-molecule fluorescence detection in microfluidic reservoirs and nanochannel regions and under nanotrap confinement. (A) The confocal detection volume was placed into the microfluidic part of the device at the mid height of the channel (i.e., 13 μm above the glass coverslip). The diffusion of multiple particles at the same time through the confocal spot results in multiple fluorescence bursts as shown in the fluorescence burst time trace. (B) The confocal fluorescence burst detection volume was placed in the nanochannel region. Fluorescence data recorded in the nanochannel shows more rare events of fluorescent bursts, which implies that the probability of multiple particles crossing the detection volume is lowered by the nanochannel confinement. (C) The detection volume was placed into the center of a nanotrap geometry. The fluorescence time trace data shows a significantly increased residence time of single particles up to tens to hundreds of milliseconds under nanotrap confinement.

to the sequential double exposure of the photoresist by UV lithography and 2PL. The central part of the array, however, shows the intended trap geometry from the prototypic procedure above with suitable traps for the confinement of the nanoparticles imprinted in PDMS. The nanochannels were 650 nm wide and connected to the nanotraps, which had a radius of 350 nm. The nanochannels and nanotraps were 750 and 650 nm in height, respectively, according to correlative profilometer measurements (Figure S2).

Single-Molecule Fluorescence Detection of Colloids and Biomolecules in Nanotraps. Single-molecule studies for biological measurements in miniaturized devices have been proven to be very useful due to their precise sample handling, small volume manipulation, and high throughput capabilities.^{40,41} Prolonged observation of single molecules or nanocolloids in solution is still a challenging task but an important step toward microfluidic total-analysis systems (μTAS).⁴² Our chip design provides an opportunity for prolonged detection of single particles in solution without permanent surface immobilization. We intend to increase particle residence times in the detection volume due to the additional local steric confinement in the nanotraps.

To demonstrate this, we performed confocal-based single-molecule burst experiments that allowed us to observe, record, and compare the events of single particles entering and leaving the nanotrapping geometry. Figure 5 schematically illustrates the experimental setup. The device's microchannel reservoirs were filled with respective particle solutions at pico- to nanomolar concentrations. Once the sample in the device

reached equilibrium and the nanoparticles started diffusing through the nanochannels, fluorescence burst detection was conducted within the nanotraps. Samples were excited with a continuous 488 nm diode laser, and their fluorescence was collected using avalanche photodiodes, which allowed readout of the fluorescent nanoparticle signal with high temporal resolution.

We first performed measurements on 40 nm fluorescent particles and compared burst detection under nanotrap confinement to residence times in the microfluidic reservoirs of the device and the nanochannel bridges. To this end, the confocal detection volume was placed in the respective region of the device, as illustrated in Figure 5A–C. Within the microfluidic part of the device (Figure 5A), multiple fluorescence burst signals overlap during the measurement and show various intensity levels due to multiple particles being able to cross through the detection volume at the same time. The time regime of transition events is in the millisecond range. In the second measurement, the laser spot was placed inside a nanochannel, as shown in Figure 5B, and confocal time traces were recorded. The number of fluorescence bursts was drastically reduced due to the single-molecule exclusion capabilities of the nanochannel, and just slightly increased detection times in comparison to measurements in the microfluidic channel were observed. Finally, we placed the confocal spot at the center of a nanotrap. Nanoparticles in a single nanotrap geometry were recorded as shown in Figure 5C. The time trace shown exemplifies the prolonged nature of

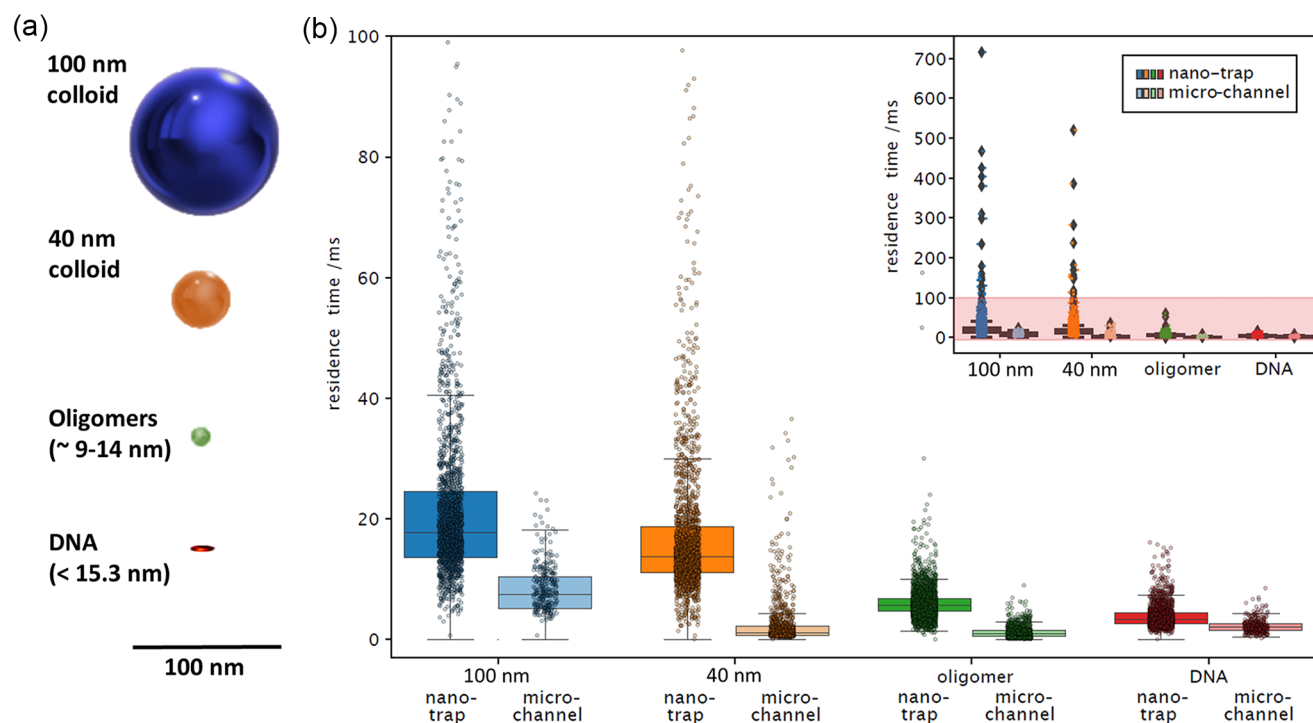


Figure 6. Residence time of specimens under nanotrap confinement. (A) Schematic illustration of the relative size difference of the probed specimens. (B) Comparison between residence times for 100 nm colloids, 40 nm colloids, α -synuclein oligomers, and 45 bp DNA in microchannel reservoirs and nanotrapping geometries. The residence time in the nanotraps relative to the detection time in the microchannel reservoirs is increased by a factor of approximately 3- to 5-fold. The inset shows the existence of rare trapping events in the hundreds of millisecond range for colloidal particles and up to tens of milliseconds for oligomers and DNA.

fluorescence burst signals obtained within a nanotrap and is common among all species under study (Figure S3).

Using the same nanofluidic geometry, we compared the behavior of differently sized particles in the nanotraps. We performed experiments, as described before, with a series of nanocolloids and biomacromolecules, including 100 nm colloids, 40 nm colloids, \sim 9–14 nm α -synuclein oligomers, and 45 bp DNA (\sim 15.3 nm length, estimated with 0.34 nm per bp, rod-like)^{43,44} in deionized water. Our results show that the nanotraps increase the residence time of the particles within the detection volume due to the additional local steric confinement. Figure 6 shows a comparison of their mean residence times inside the nanotraps in relation to the microfluidic channels. The time spent by the particle inside the laser spot depends on its diffusional properties and therefore on its size. In general, according to the Stokes–Einstein relation, the diffusion coefficient is defined as $D = (k_B T) / (6\pi\eta R_H)$, where R_H is the hydrodynamic radius, k_B is the Boltzmann constant, T is the temperature, and η is the viscosity. This trend can be observed for confined and nonconfined particles. Strikingly, the comparison of the nanotrap residence time to the microfluidic channel indicates an up to 5-fold increase of observation time within the confocal detection volume. This is expected because the walls limit the possibility of the molecule escaping from the laser's field of view, as mentioned above. The Debye length can be assumed to be less than 100 nm⁴⁵ and should not be the major factor in the confinement presented here, but it definitely needs to be considered when using smaller nanofluidic design dimensions. The enhancement of the residence time, once the particle is in the nanotrap, thus enables the longer signal capture of a single particle. This opens up the possibility for single-molecule

metrology of biomolecules and colloids in solution over extended periods of time.

CONCLUSIONS

In this paper, we have demonstrated the use of hybrid 2PL for the fabrication of nanotraps written adjacent to nanofluidic and microfluidic channels and their usage for the study of colloidal nanoparticles and biomacromolecules at the single-molecule level. We have established conditions for the successful generation of a silicon master wafer with nanoconfinement geometries in a negative SU-8 photoresist by combining 2-photon direct laser writing with UV lithography. We imprinted nanofluidic devices from the silicon master wafer into PDMS to make functional nanochannels with adjacent nanotraps of 350 nm radius and 650 nm height, but also, much smaller geometries and structures below 100 nm in height are possible (Figure S1). Given the ease of fabrication, our approach can be readily adopted by laboratories with access to commercial or custom-built 2PL systems and allows for the fabrication and prototyping in a high-throughput and scalable manner as opposed to EBL and sequential clean room nanofabrication techniques.

To demonstrate the applicability of the nanotrapping devices developed herein for the prolonged observation of single molecules, we used single-particle fluorescence burst detection to measure the residence time of polymer nanoparticles such as 100 and 40 nm colloids and various biological relevant samples like α -synuclein oligomers and fluorescently labeled 45 bp DNA in nanofluidic confinements. Although our nanotrap geometry is orders of magnitude larger in comparison to the biological specimen under study, we observed a significant increase in residence times of the samples. All species analyzed

in the same trapping geometry showed up to a 3- or 5-fold increase of observation time in a diffraction limited confocal detection volume. This finding is significant, as it opens up the possibility to study and analyze biomacromolecules or biomolecular assemblies in solution without permanent surface immobilization for extended periods of time. It also allows a longer observation of the same molecule for optical techniques that greatly benefit from higher photon counts such as Förster resonance energy transfer (FRET) measurements at the single-molecule level.

Readout is not limited to single-particle fluorescence burst detection. As a proof of concept, we also explored other fluorescence microscopy techniques (confocal imaging and TIRF microscopy) as alternative readout techniques to be used in combination with nanofluidics (Figures S4 and S5). This gives laboratories guidance on how to use nanotrapping devices with their already available fluorescence microscopy equipment according to their needs and research applications. This highlights the versatility of the applications that can be envisaged with our nanofluidic device in conjunction with different optical modalities. We anticipate that the cost-effective and easy approach for fabrication of nanofluidic devices has the potential to find broad applicability in various applications in the nanobiotechnologies, biophysics, and clinical diagnostics. Researchers interested in topics such as the synthesis and functionalization of nanoparticles for nanomedicine and drug delivery,⁴⁶ metal–organic frameworks,⁴⁷ guest–host complexes,⁴⁸ carbon quantum dots,⁴⁹ bottom-up assembled meta materials (e.g., gold nanocubes, gold nanoparticles),⁷ active colloids⁵⁰ (e.g., Janus particles), or general spectroscopic analysis of light–matter interactions in solution⁵¹ (e.g., Raman spectroscopy, second-harmonic generation (SHG), nonlinear refractive indices, FRET) would greatly benefit from the approach presented here.

Similar nanofluidic devices were previously established by Krishnan et al. for the geometry-induced electrostatic trapping of nanocolloids,²² where iSCAT provided a label-free readout method of gold nanoparticle and liposome residence times in the nanoconfinement. The silica-based devices were fabricated using RIE etching, and the method involves several clean room fabrication steps; therefore, it is not easily prototyped by biological laboratories with limited access to nanofabrication facilities. An important step to make this technology more available to the research community was achieved by Gerspach et al.⁵² who molded electrostatic trapping devices in PDMS and measured the residence time of highly charged gold nanoparticles of 60, 80, and 100 nm diameter in the nanopockets. Their experiments showed that confinement is highly dependent on the size ratio between the particle and the trap, which underlines the importance of flexible fabrication schemes that can adapt to the application accordingly.

In contrast, the method demonstrated in the present paper shows the advantage of a stationary chip design without external machinery to study a variety of biological specimens from colloids to oligomers and DNA molecules in confined space without permanently immobilizing or perturbing them. EBL and RIE as the golden standards for the fabrication of silica trapping devices have higher lateral resolution than 2PL, but 2PL allows a more versatile integration of complex nanofluidic and nanotrapping geometries into microfluidic device platforms in the submicron regime.

Taken together, in this paper, we give a cost-effective and facile approach for the fabrication of nanofluidic devices to

study single molecules in solution without permanent surface immobilization using hybrid 2-photon lithography. With our approach, we envisage the facilitation of nanoparticle trapping technology in biological and biomedical laboratories, paving the way for the use of photon-intensive spectroscopic techniques for applications related to protein misfolding disease, cancer research, and bionanotechnology.

METHODS

Wafer Preparation and Development. SU-8 photoresist (Type 3025, Micro Resist Technology) was spin coated (Laurell Technologies, WS-650) at 3000 rpm onto a 3 in. silicon wafer (MicroChemicals, Prime CZ-Si, thickness of $381 \pm 20 \mu\text{m}$, polished, p-type) to a height of $25 \mu\text{m}$. The SU-8 coated wafer was soft baked and treated according to the protocol of the supplier of the photoresist. Microfluidic patterns from a custom-designed film mask (Microlithography) were then projected onto the wafer, and the photoresist was exposed for 30 s to the UV-LED setup as described in Challa et al.⁵³ The wafer was postbaked at $95 \text{ }^\circ\text{C}$ so that the interfaces between exposed and unexposed regions became visible due to their change in refractive index, which assisted in alignment of the microstructures with the 2PL setup. After, the nanostructures were written with 2PL and the wafer baked at $95 \text{ }^\circ\text{C}$ for 8 min. The wafer was developed using propylene glycol monomethyl ether acetate (PGMEA) (Sigma-Aldrich) and subsequently given a second exposure to UV light for 30 s to make structures mechanically stable on the wafer before final rinsing of the structures with PGMEA and isopropanol (IPA) (Sigma-Aldrich).³⁹ A postbake of 30 min at $95 \text{ }^\circ\text{C}$ on a hot plate was done at the end of the development process to increase mechanical stability of the nanostructures.

2-Photon Lithography. A custom-built 2PL setup was used to write the calibration patterns as well as the final nanofluidic master mold. A detailed description of the upright 2-photon lithography setup and its fabrication capabilities can be found in Vanderpoorten et al.³² Briefly, the system uses a femtosecond fiber laser (Menlo System C Fiber 780 HP) modulated as the first diffraction order of an acousto-optic modulator (AA Optoelectronics). The beam is widened through a beam expander (Thorlabs, BE02-05-B) and led over a 90:10 R:T beamsplitter (BS028, Thorlabs) into a microscope objective vertically mounted above the sample. Reflected light is collected with a tube lens (Thorlabs AC 254-100-A-ML, BBAR coating A OM 31 400–700 nm, $f = 100.0 \text{ mm}$) onto a camera ($\mu\text{Eye ML}$, Industry camera, USB 3.0). An optical electromechanical shutter (Thorlabs, SHB1) is mounted in front of the camera to protect it during high power laser writing. Through an additional 30:70 (R:T) beam splitter (BS019, Thorlabs) in the camera detection arm, a white LED (Thorlabs, MCWHL5) allows nonpolymerizing inspection of the sample in wide field. A 3 in. wafer coated with prebaked SU-8 ($25 \mu\text{m}$ thickness) was immobilized on a PI Nanocube (P-611.3S, Physikalische Instrumente) mounted on two perpendicular stacked motorized linear-precision stages (M-404.2PD, Physikalische Instrumente, Ball screw, 80 mm wide, ActiveDrive). Immersion Oil (Cargille laboratories, LDF, Code 387) was added onto the SU-8 layer before manually bringing the oil immersion objective (Leica, 63 \times , PL APO, 1.40 NA) in close proximity to the wafer surface. The oil used here showed no reaction with unpolymerized SU-8 photo resin and facilitated easy and scalable two-photon printing. Custom-written software then automatically focuses on the wafer surface, corrects for tilt, and coordinates the interplay of piezo, translational stages and laser power modulation to write the intended patterns. The laser beam intensity of the writing beam was directly measured after the acousto-optic modulator using a power meter (Thorlabs, S310C, thermal power head). To prevent exposure of the resin during the focusing process, the laser power was kept below the polymerization threshold but high enough to be detected on the system's camera. The full travel range of the nanocube of $100 \mu\text{m} \times 100 \mu\text{m}$ was used to write a calibration array of lines and dots. Then, the motorized stages were used to displace the piezo scanning areas and write a new pattern (e.g., $300 \mu\text{m}$ displacement, positional precision = $1 \mu\text{m}$) with

adapted parameters. The positioning repeatability of the piezo actor (Nanocube) was below 10 nm according to the manufacturer and is key for automated focusing and reliable nanofabrication. For 2-photon writing in the microfluidic master, we used a white light LED to first place the laser focus in between the two microchannels and then started the automated laser writing process. The system uses the autofocus function each time it adds another nanofluidic array. This allows stepwise but precise addition of nanofluidic features on the wafer scale.

Correlative Scanning Electron Microscopy and Atomic Force Microscopy Imaging. After the development process of the 2-photon written calibration assay, the wafer was manually cut into smaller dimensions to allow easier sample handling. Imprints of the master wafer were taken following conventional soft lithography protocols with a 10:1 PDMS (Sylgard 184)/curing agent ratio. After PDMS curing, the area of interest was cut out using a surgical scalpel. The PDMS imprint was coated with 10 nm of platinum (Quorum Technologies Q150T ES Turbo-Pumped Sputter Coater/Carbon Coater) and imaged using a commercial SEM (TESCAN MIRA3 FEG-SEM). The original SU-8 features were coated with a layer of 10 nm platinum as well and imaged on the same SEM in order to compare the imprinted features with the original molds. The final nanofluidic PDMS device imprint was imaged following the same procedures and on the same microscope. AFM was conducted on the calibration sample using a Park Systems NX10 AFM. According to previous findings by Cabrera et al.,⁵⁴ the PDMS surface roughness can be assumed to be below 5 nm, which should therefore not influence the steric trapping behavior significantly.

Profilometer Measurements of Nanotraps. The 2-photon written nanofluidic master wafer was cleaned using pressurized air and placed in a profilometer (KLA Corporation, Tencor P-6) for height measurements of the nanochannels and nanotraps. Using the integrated microscope of the system, the scan direction was aligned along the center of a nanotrapping array located between the two microfluidic reservoirs. The sample was scanned at a speed of 2.00 $\mu\text{m/s}$ with a height scan rate of 500 Hz and a force of 0.5 mg applied using a 2.00 μm (diameter) tip.

Single-Molecule Confocal Measurements. Single-molecule fluorescence measurements were performed on a custom-built single-molecule confocal microscope. Nanofluidic PDMS–silica devices were secured to a motorized microscope stage (Applied Scientific Instrumentation, PZ-2000FT). The sample was excited using a 488 nm wavelength laser (Cobolt 06-MLD, 200 mW diode laser, Cobolt), which was directed to the back aperture of a 60 \times magnification water-immersion objective (CFI Plan Apochromat WI 60 \times , NA 1.2, Nikon) using a single-mode optical fiber (P3-488PM-FC-1, Thorlabs) and an achromatic fiber collimator (60FC-L-4-M100S-26, Schäfter/Kirchhoff GmbH). The laser intensity at the back aperture of the objective was adjusted to 150 μW . The laser beam exiting the optical fiber was reflected by a dichroic mirror (Di03-R488/561, Semrock), directed to the objective, and focused into the chip to a diffraction-limited confocal spot. The motorized stage was used to position the confocal spot within the chip. The emitted light from the sample was collected through the same objective and dichroic mirror and then passed through a 30 μm pinhole (Thorlabs) to remove any out-of-focus light. The emitted photons were filtered through a band-pass filter (FF01-520/35-25, Semrock) and then focused onto an avalanche photodiode (APD; SPCM-14, PerkinElmer Optoelectronics) connected to a Time-Harp260 time-correlated single-photon counting unit (PicoQuant). Photon time traces were recorded using the SymPhoTime 64 software package (Picoquant) with a binning time of 1 ms.

Preparation of Labeled α -Synuclein Oligomers. The N122C variant of α -synuclein was purified into phosphate buffered saline (PBS; pH 7.4) as described previously⁵⁵ with the addition of 3 mM DTT to all buffers to prevent dimerization. Following removal of DTT from the purified monomers by a PD10 desalting column packed with a Sephadex G25 matrix (GE Healthcare), the protein was incubated with a 1.5-fold molar excess of Alexa488 with a maleimide linker (ThermoFisher Scientific) (overnight, 4 $^{\circ}\text{C}$ on a rolling

system). In order to remove the free dye, the mixture was subsequently subjected to size exclusion chromatography using a Superdex 200 16/600 (GE Healthcare) and eluted in PBS (pH 7.4) at 20 $^{\circ}\text{C}$. Protein fractions were pooled, and the Alexa488 labeled α -synuclein concentration was estimated by dye absorbance, assuming 1:1 dye/protein stoichiometry (72 000 L/mol cm at 495 nm). Stable α -synuclein oligomers were formed from Alexa488 labeled monomers as previously described.⁵⁶ Briefly, monomeric α -synuclein was lyophilized in Milli-Q water and resuspended in PBS (pH 7.4) at a concentration of 12 mg/mL. Following incubation (37 $^{\circ}\text{C}$, 20–24 h), the samples were ultracentrifuged (1 h, 288 000g) (Optima TLX Ultracentrifuge, Beckman Coulter, TLA-120.2 Beckman rotor) to remove large aggregates. Monomeric protein was removed by multiple filtration steps through 100 kDa concentrating filters. The oligomer concentration was estimated on the basis of the dye absorbance (72 000 L/mol cm at 495 nm).

Sample and Device Preparation for Single-Molecule Experiments. 100 and 40 nm fluorescent colloids (FluoSpheres) were purchased from ThermoFisher. α -Synuclein oligomers were prepared as described above. Double-stranded DNA was prepared from two single-stranded DNA oligonucleotides by thermal annealing. Oligonucleotides were synthesized and labeled by Biomers. The sequences were 5'-GCC TTA TTT TCA CTC TTT CCT TTC TTC TTC TCT CTT TTT TTC CCG-3' (top strand) and 5'-CGG GAA AAA AAG AGA GAA GAA GAA AGG AAA GAG TGA AAA TAA GGC-3' (bottom strand); the top strand was labeled with Atto488 at the thymidine at position 7, shown in bold type.

Micro/nanofluidic devices were molded from the fabricated SU-8 master via soft lithography using PDMS (Sylgard 184, with a 10:1 curing agent ratio). After baking, inlets were added using surgical punchers and plasma bonded to coverslip glasses (Menzel coverslips, grade H1.5). The surface of the coverslips and the PDMS were plasma treated and, afterward, manually pressed on top of each other. Devices were used directly after the plasma bonding step to use their remaining surface hydrophilicity for easier filling of the devices. Before the experiments, the chips were filled by pipetting equal amounts of diluted sample solutions into the inlet areas and equilibrated for 20 min.

■ ASSOCIATED CONTENT

SI Supporting Information

The Supporting Information is available free of charge at <https://pubs.acs.org/doi/10.1021/acsanm.1c03691>.

Additional surface structure analysis and image data acquired by AFM on a 2p-fabricated nanotrap master wafer (SU-8 on silicon); profilometer data of the master wafer used for confocal fluorescence burst detection experiments; comparative figure of fluorescence burst traces of 100 nm colloids, oligomers, and 40 bp DNA; experimental description of confocal microscopy and TIRF imaging for 100 and 40 nm particle detection in nanotraps; images, kymographs, and traces acquired using formerly mentioned fluorescence microscopy imaging techniques (PDF)

■ AUTHOR INFORMATION

Corresponding Author

Tuomas P. J. Knowles – Yusuf Hamied Department of Chemistry, University of Cambridge, Cambridge CB2 1EW, United Kingdom; Cavendish Laboratory, Department of Physics, University of Cambridge, Cambridge CB30HE, United Kingdom; orcid.org/0000-0002-7879-0140; Email: tpjk2@cam.ac.uk

Authors

Oliver Vanderpoorten – Yusuf Hamied Department of Chemistry, University of Cambridge, Cambridge CB2 1EW, United Kingdom; Department of Chemical Engineering and Biotechnology, University of Cambridge, Cambridge CB3 0AS, United Kingdom; Cavendish Laboratory, Department of Physics, University of Cambridge, Cambridge CB30HE, United Kingdom; Department of Physics and Technology, UiT The Arctic University of Norway, Tromsø 9019, Norway; orcid.org/0000-0001-5611-470X

Ali N. Babar – Yusuf Hamied Department of Chemistry, University of Cambridge, Cambridge CB2 1EW, United Kingdom; Cavendish Laboratory, Department of Physics, University of Cambridge, Cambridge CB30HE, United Kingdom

Georg Krainer – Yusuf Hamied Department of Chemistry, University of Cambridge, Cambridge CB2 1EW, United Kingdom; orcid.org/0000-0002-9626-7636

Raphaël P. B. Jacquat – Yusuf Hamied Department of Chemistry, University of Cambridge, Cambridge CB2 1EW, United Kingdom

Pavan K. Challa – Yusuf Hamied Department of Chemistry, University of Cambridge, Cambridge CB2 1EW, United Kingdom; orcid.org/0000-0002-0863-381X

Quentin Peter – Yusuf Hamied Department of Chemistry, University of Cambridge, Cambridge CB2 1EW, United Kingdom; orcid.org/0000-0002-8018-3059

Zenon Toprakcioglu – Yusuf Hamied Department of Chemistry, University of Cambridge, Cambridge CB2 1EW, United Kingdom; orcid.org/0000-0003-1964-8432

Catherine K. Xu – Yusuf Hamied Department of Chemistry, University of Cambridge, Cambridge CB2 1EW, United Kingdom

Ulrich F. Keyser – Cavendish Laboratory, Department of Physics, University of Cambridge, Cambridge CB30HE, United Kingdom; orcid.org/0000-0003-3188-5414

Jeremy J. Baumberg – Cavendish Laboratory, Department of Physics, University of Cambridge, Cambridge CB30HE, United Kingdom; orcid.org/0000-0002-9606-9488

Clemens F. Kaminski – Department of Chemical Engineering and Biotechnology, University of Cambridge, Cambridge CB3 0AS, United Kingdom; orcid.org/0000-0002-5194-0962

Complete contact information is available at:
<https://pubs.acs.org/10.1021/acsanm.1c03691>

Author Contributions

[†]O.V., A.N.B., G.K., and R.P.B.J. contributed equally to this work. O.V. and A.N.B. fabricated the nanofluidic masters and chips using two-photon lithography. A.N.B. characterized the calibration assays using SEM and AFM. O.V. conducted profilometer measurements on the nanofluidic master wafer. G.K. built the confocal burst detection setup and conducted the fluorescence burst experiments of the colloids, oligomers, and DNA in the nanotrap devices and microchannels. O.V. and A.N.B. imaged trapping events of the colloidal particles using confocal microscopy. P.K.C., Z.T., A.N.B., and O.V. conducted TIRF microscopy measurements of the colloidal particles. P.K.C. and Z.T. also conducted trapping experiments using conventional UV lithography in an early stage of the project, which helped form the content of this paper. R.P.B.J. contributed to data analysis and wrote the software for the residence time measurements of the fluorescence burst data. Q.P. improved the control software of the two-photon system,

which allowed us to run the initial tests and conduct the fabrication assay. C.K.X. prepared and purified the oligomer samples used for all the experiments. O.V., G.K., and A.N.B. wrote the paper. All authors provided input into the manuscript with significant contributions and guidance of U.F.K., J.J.B., C.F.K., and T.P.J.K.

Notes

The authors declare no competing financial interest.

ACKNOWLEDGMENTS

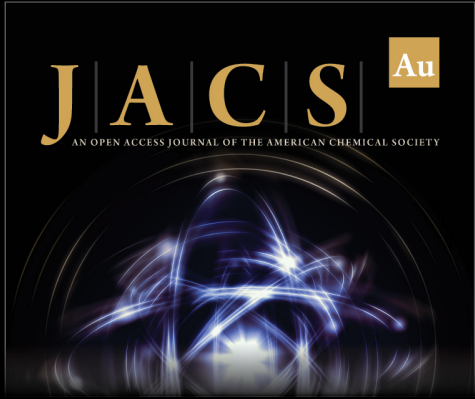
The work was funded by the Horizon 2020 programme through 766972-FET-OPEN-NANOPHLOW (T.P.J.K.). The research leading to these results has further received funding from the European Research Council under the European Union's Horizon 2020 Framework Programme through the Marie Skłodowska-Curie grant MicroSPARK (agreement no. 841466; G.K.), the Herchel Smith Funds (G.K.), and the Wolfson College Junior Research Fellowship (G.K.). This work was also supported by the Engineering and Physical Sciences Research Council [grant number EP/L015889/1]. The authors would also like to thank the NanoDTC for additional funding and the Maxwell Community for scientific support.

REFERENCES

- (1) Gao, D.; Ding, W.; Nieto-Vesperina, S. M.; Ding, X.; Rahman, M.; Zhang, T. C.; Lim, C.; Qiu, C. W. Optical manipulation from the microscale to the nanoscale: fundamentals, advances and prospects. *Light: Sci. Appl.* **2017**, *6* (9), e17039–e17039.
- (2) Wang, Q.; Goldsmith, R. H.; Jiang, Y.; Bockenhauer, S. D.; Moerner, W. E. Probing single biomolecules in solution using the anti-brownian electrokinetic (ABEL) trap. *Acc. Chem. Res.* **2012**, *45* (11), 1955–1964.
- (3) Huang, T.; Deng, C. X. Current Progresses of Exosomes as Cancer Diagnostic and Prognostic Biomarkers. *Int. J. Biol. Sci.* **2019**, *15* (1), 1–11.
- (4) Squires, A. H.; Dahlberg, P. D.; Liu, H.; Magdaong, N. C. M.; Blankenship, R. E.; Moerner, W. E. Single-molecule trapping and spectroscopy reveals photophysical heterogeneity of phycobilisomes quenched by Orange Carotenoid Protein. *Nat. Commun.* **2019**, *10* (1), 1–12.
- (5) Squires, A. H.; Lavania, A. A.; Dahlberg, P. D.; Moerner, W. E. Interferometric Scattering Enables Fluorescence-Free Electrokinetic Trapping of Single Nanoparticles in Free Solution. *Nano Lett.* **2019**, *19* (6), 4112–4117.
- (6) Cohen, A. E.; Moerner, W. E. Method for trapping and manipulating nanoscale objects in solution. *Appl. Phys. Lett.* **2005**, *86* (9), 093109.
- (7) Mann, M. E.; Yadav, P.; Kim, S. Colloidal Plasmonic Nanocubes as Capacitor Building Blocks for Multidimensional Optical Metamaterials: A Review. *ACS Appl. Nano Mater.* **2021**, *4* (10), 9976–9984.
- (8) Ke, P. C.; Zhou, R.; Serpell, L. C.; Riek, R.; Knowles, T. P. J.; Lashuel, H. A.; Gazit, E.; Hamley, I. W.; Davis, T. P.; Fändrich, M.; Otzen, D. E.; Chapman, M. R.; Dobson, C. M.; Eisenberg, D. S.; Mezzenga, R. Half a century of amyloids: past, present and future. *Chem. Soc. Rev.* **2020**, *49* (15), 5473–5509.
- (9) Endo, M.; Yang, Y.; Sugiyama, H. DNA origami technology for biomaterials applications. *Biomater. Sci.* **2013**, *1*, 347–360.
- (10) Barzegar Amiri Olia, M.; Donnelly, P. S.; Hollenberg, L. C. L.; Mulvaney, P.; Simpson, D. A. Advances in the Surface Functionalization of Nanodiamonds for Biological Applications: A Review. *ACS Appl. Nano Mater.* **2021**, *4* (10), 9985–10005.
- (11) Roy, R.; Hohng, S.; Ha, T. A practical guide to single-molecule FRET. *Nat. Methods* **2008**, *5* (6), 507–516.

- (12) Grasso, L.; Wyss, R.; Weidenauer, L.; Thampi, A.; Demurtas, D.; Prudent, M.; Lion, N.; Vogel, H. Molecular screening of cancer-derived exosomes by surface plasmon resonance spectroscopy. *Anal. Bioanal. Chem.* **2015**, *407* (18), 5425–5432.
- (13) Choi, U. B.; Weninger, K. R.; Bowen, M. E. Immobilization of proteins for single-molecule fluorescence resonance energy transfer measurements of conformation and dynamics. *Methods Mol. Biol.* **2012**, *896*, 3–20.
- (14) Yang, H. Y.; Moerner, W. E. Resolving Mixtures in Solution by Single-Molecule Rotational Diffusivity. *Nano Lett.* **2018**, *18* (8), 5279–5287.
- (15) Tanyeri, M.; Schroeder, C. M. Manipulation and Confinement of Single Particles Using Fluid Flow. *Nano Lett.* **2013**, *13* (6), 2357–2364.
- (16) Bradac, C. Nanoscale Optical Trapping: A Review. *Adv. Opt. Mater.* **2018**, *6* (12), 1800005.
- (17) Chen, C.; Juan, M. L.; Li, Y.; Maes, G.; Borghs, G.; Van Dorpe, P.; Quidant, R. Enhanced optical trapping and arrangement of nano-objects in a plasmonic nanocavity. *Nano Lett.* **2012**, *12* (1), 125–132.
- (18) Melzer, J. E.; McLeod, E. Fundamental Limits of Optical Tweezer Nanoparticle Manipulation Speeds. *ACS Nano* **2018**, *12* (3), 2440–2447.
- (19) Hill, E. H.; Li, J.; Lin, L.; Liu, Y.; Zheng, Y. Opto-Thermophoretic Attraction, Trapping, and Dynamic Manipulation of Lipid Vesicles. *Langmuir* **2018**, *34* (44), 13252–13262.
- (20) Chen, J.; Cong, H.; Loo, F. C.; Kang, Z.; Tang, M.; Zhang, H.; Wu, S. Y.; Kong, S. K.; Ho, H. P. Thermal gradient induced tweezers for the manipulation of particles and cells. *Sci. Rep.* **2016**, *6*, 35814.
- (21) Wang, K.; Schonbrun, E.; Steinvurzel, P.; Crozier, K. B. Trapping and rotating nanoparticles using a plasmonic nano-tweezer with an integrated heat sink. *Nat. Commun.* **2011**, *2* (1), 469.
- (22) Krishnan, M.; Mojarad, N.; Kukura, P.; Sandoghdar, V. Geometry-induced electrostatic trapping of nanometric objects in a fluid. *Nature* **2010**, *467* (7316), 692–695.
- (23) Krishnan, M. Electrostatic free energy for a confined nanoscale object in a fluid. *J. Chem. Phys.* **2013**, *138* (11), 114906.
- (24) Bernalova, M. I.; Mahanta, S.; Krishnan, M. Single-molecule trapping and measurement in solution. *Curr. Opin. Chem. Biol.* **2019**, *51*, 113–121.
- (25) Mojarad, N.; Krishnan, M. Measuring the size and charge of single nanoscale objects in solution using an electrostatic fluidic trap. *Nat. Nanotechnol.* **2012**, *7* (7), 448–452.
- (26) Ruggeri, F.; Krishnan, M. Entropic Trapping of a Singly Charged Molecule in Solution. *Nano Lett.* **2018**, *18* (6), 3773–3779.
- (27) Ruggeri, F.; Zosel, F.; Mutter, N.; Rózycka, M.; Wojtas, M.; Ozyhar, A.; Schuler, B.; Krishnan, M. Single-molecule electrometry. *Nat. Nanotechnol.* **2017**, *12* (5), 488–495.
- (28) Duan, C.; Wang, W.; Xie, Q. Review article: Fabrication of nanofluidic devices. *Biomicrofluidics* **2013**, *7* (2), 026501.
- (29) Menard, L. D.; Ramsey, J. M. Electrokinetically-driven transport of DNA through focused ion beam milled nanofluidic channels. *Anal. Chem.* **2013**, *85* (2), 1146–1153.
- (30) Bruno, G.; Di Trani, N. D.; Hood, R. L.; Zabre, E.; Filgueira, C. S.; Canavese, G.; Jain, P.; Smith, Z.; Demarchi, D.; Hosali, S.; Pimpinelli, A.; Ferrari, M.; Grattoni, A. Unexpected behaviors in molecular transport through size-controlled nanochannels down to the ultra-nanoscale. *Nat. Commun.* **2018**, *9* (1), 1682.
- (31) Maruo, S.; Nakamura, O.; Kawata, S. Three-dimensional microfabrication with two-photon-absorbed photopolymerization. *Opt. Lett.* **1997**, *22* (2), 132.
- (32) Vanderpoorten, O.; Peter, Q.; Challa, P. K.; Keyser, U. F.; Baumberg, J. J.; Kaminski, C. F.; Knowles, T. P. J. Scalable integration of nano-, and microfluidics with hybrid two-photon lithography. *Microsyst. Nanoeng.* **2019**, *5* (1), 1–9.
- (33) Barner-Kowollik, C.; Bastmeyer, M.; Blasco, E.; Delaittre, G.; Müller, P.; Richter, B.; Wegener, M. 3D Laser Micro- and Nanoprinting: Challenges for Chemistry. *Angew. Chem., Int. Ed.* **2017**, *56* (50), 15828–15845.
- (34) Zhou, X.; Hou, Y.; Lin, J. A review on the processing accuracy of two-photon polymerization. *AIP Adv.* **2015**, *5* (3), 030701.
- (35) Oellers, M.; Lucklum, F.; Vellekoop, M. J. On-chip mixing of liquids with swap structures written by two-photon polymerization. *Microfluid. Nanofluid.* **2020**, *24* (1), 4.
- (36) Venkatakrishnan, K.; Jariwala, S.; Tan, B. Maskless fabrication of nano-fluidic channels by two-photon absorption (TPA) polymerization of SU-8 on glass substrate. *Opt. Express* **2009**, *17* (4), 2756.
- (37) Sugioka, K.; Xu, J.; Wu, D.; Hanada, Y.; Wang, Z.; Cheng, Y.; Midorikawa, K. Femtosecond laser 3D micromachining: A powerful tool for the fabrication of microfluidic, optofluidic, and electrofluidic devices based on glass. *Lab Chip* **2014**, *14* (18), 3447–3458.
- (38) Xia, Y.; Whitesides, G. M. Soft lithography. *Annu. Rev. Mater. Sci.* **1998**, *28*, 153.
- (39) Purto, J.; Verch, A.; Rogin, P.; Hensel, R. Improved development procedure to enhance the stability of microstructures created by two-photon polymerization. *Microelectron. Eng.* **2018**, *194*, 45–50.
- (40) Whitesides, G. M. The origins and the future of microfluidics. *Nature* **2006**, *442* (7101), 368–373.
- (41) Streets, A. M.; Huang, Y. Microfluidics for biological measurements with single-molecule resolution. *Curr. Opin. Biotechnol.* **2014**, *25*, 69–77.
- (42) Guijt, R. M.; Manz, A. Miniaturised total chemical-analysis systems (MTAS) that periodically convert chemical into electronic information. *Sens. Actuators, B* **2018**, *273*, 1334–1345.
- (43) Castro, C. E.; Kilchherr, F.; Kim, D. N.; Shiao, E. L.; Wauer, T.; Wortmann, P.; Bathe, M.; Dietz, H. A primer to scaffolded DNA origami. *Nat. Methods* **2011**, *8* (3), 221–229.
- (44) Guilbaud, S.; Salomé, L.; Destainville, N.; Manghi, M.; Tardin, C. Dependence of DNA Persistence Length on Ionic Strength and Ion Type. *Phys. Rev. Lett.* **2019**, *122* (2), 028102.
- (45) Schoch, R. B.; Han, J.; Renaud, P. Transport phenomena in nanofluidics. *Rev. Mod. Phys.* **2008**, *80*, 839.
- (46) Doane, T. L.; Burda, C. The unique role of nanoparticles in nanomedicine: imaging, drug delivery and therapy. *Chem. Soc. Rev.* **2012**, *41* (7), 2885–2911.
- (47) Jhang, W. L.; Huang, M. S.; Hsu, S. W. Unsymmetrical Heterogeneous Au-Ag Nanocrystals as Catalysts, Sensors, and Drug Carriers. *ACS Appl. Nano Mater.* **2021**, *4* (10), 10011–10017.
- (48) Xiong, T.; Zhang, Y.; Donà, L.; Gutiérrez, M.; Möslin, A. F.; Babal, A. S.; Amin, N.; Civalleri, B.; Tan, J. C. Tunable Fluorescein-Encapsulated Zeolitic Imidazolate Framework-8 Nanoparticles for Solid-State Lighting. *ACS Appl. Nano Mater.* **2021**, *4* (10), 10321–10333.
- (49) Lim, S. Y.; Shen, W.; Gao, Z. Carbon quantum dots and their applications. *Chem. Soc. Rev.* **2015**, *44* (1), 362–381.
- (50) Wang, Z.; Wang, Z.; Li, J.; Tian, C.; Wang, Y. Active colloidal molecules assembled via selective and directional bonds. *Nat. Commun.* **2020**, *11* (1), 1–12.
- (51) Huang, T. C.; Tsai, H. C.; Chin, Y. C.; Huang, W. S.; Chiu, Y. C.; Hsu, T. C.; Chia, Z. C.; Hung, T. C.; Huang, C. C.; Hsieh, Y. T. Concave Double-Walled AgAuPd Nanocubes for Surface-Enhanced Raman Spectroscopy Detection and Catalysis Applications. *ACS Appl. Nano Mater.* **2021**, *4* (10), 10103–10115.
- (52) Gerspach, M. A.; Mojarad, N.; Sharma, D.; Pfohl, T.; Ekinci, Y. Soft electrostatic trapping in nanofluidics. *Microsystems Nanoeng.* **2017**, *3* (1), 17051.
- (53) Challa, P. K.; Kartanas, T.; Charmet, J.; Knowles, T. P. J. Microfluidic devices fabricated using fast wafer-scale LED-lithography patterning. *Biomicrofluidics* **2017**, *11*, 014113.
- (54) Cabrera, J. N.; Ruiz, M. M.; Fascio, M.; D'Accorso, N.; Mincheva, R.; Dubois, P.; Lizarraga, L.; Negri, R. M. Increased Surface Roughness in Polydimethylsiloxane Films by Physical and Chemical Methods. *Polymers (Basel, Switz.)* **2017**, *9* (8), 331.
- (55) Hoyer, W.; Antony, T.; Cherny, D.; Heim, G.; Jovin, T. M.; Subramaniam, V. Dependence of α -synuclein aggregate morphology on solution conditions. *J. Mol. Biol.* **2002**, *322* (2), 383–393.

(56) Chen, S. W.; Drakulic, S.; Deas, E.; Ouberai, M.; Aprile, F. A.; Arranz, R.; Ness, S.; Roodveldt, C.; Williams, T.; De-Genst, E. J.; Klenerman, D.; Wood, N. W.; Knowles, T. P. J.; Alfonso, C.; Rivas, G.; Abramov, A. Y.; Valpuesta, J. M.; Dobson, C. M.; Cremades, N. Structural characterization of toxic oligomers that are kinetically trapped during α -synuclein fibril formation. *Proc. Natl. Acad. Sci. U. S. A.* **2015**, *112* (16), E1994–E2003.



The image shows the cover of the journal JACS Au. The title "JACS Au" is prominently displayed in gold serif font, with "Au" in a smaller gold box. Below the title, it reads "AN OPEN ACCESS JOURNAL OF THE AMERICAN CHEMICAL SOCIETY". The central graphic is a glowing blue and white molecular structure or network of light trails. Below the graphic is a small portrait of Prof. Christopher W. Jones, followed by his name and title: "Editor-in-Chief Prof. Christopher W. Jones, Georgia Institute of Technology, USA". At the bottom, there is a gold banner that says "Open for Submissions" with a padlock icon. The ACS Publications logo and tagline "Most Trusted. Most Cited. Most Read." are at the bottom right. The website "pubs.acs.org/jacsau" is at the bottom left.

pubs.acs.org/jacsau

Editor-in-Chief
Prof. Christopher W. Jones
Georgia Institute of Technology, USA

Open for Submissions 

ACS Publications
Most Trusted. Most Cited. Most Read.